polymer papers

Three-dimensional study of cylindrical morphology in a styrene–butadiene–styrene block copolymer

Richard J. Spontak and Michael C. Williams
Center for Advanced Materials, Lawrence Berkeley Laboratory, and Department of Chemical Engineering, University of California, Berkeley, CA 94720-9989, USA

and David A. Agard
Department of Biochemistry and Biophysics, University of California, San Francisco, CA 94143-0448, USA
(Received 6 July 1987; revised 31 August 1987; accepted 7 September 1987)

When a block copolymer undergoes microphase separation, well ordered microstructures result which give the copolymer unique thermal and mechanical properties. In relating these properties quantitatively to the microstructure, and in devising models for the phase separation, theoreticians have always invoked highly idealized structural elements. However, variations in the actual microstructure may also play a significant role in these properties, so we describe here a method for highly detailed examination of these elements. By using transmission electron microscopy (TEM), we have obtained projections of a styrene–butadiene–styrene (SBS) copolymer (30 wt % styrene) at tilt angles ranging from $-61.5°$ to $+48.5°$ in 5° increments. Applying a filtered back-projection reconstruction method to this set of tilted projections yielded a three-dimensional view of the polymer, revealing two different types of structures. The first type resembled cylinders in hexagonal packing with some deviations from geometric ideality. In these cases, the microstructures were found to extend through the thickness of the TEM sample (approximately 36 nm) and were oriented normal to the surface. In the second type of structure, globules of polystyrene were observed in a clearly non-equilibrium condition. Qualitative information concerning the evolutionary process of cylindrical domain formation was obtained from the shapes of these globules.

(Keywords: block copolymers; microstructure; electron microscopy)

INTRODUCTION

Microstructures on the size scale of polymer chains result when block copolymers undergo microphase separation due to thermodynamic incompatibility of the blocks. The microstructural elements, rich in one block component, take the form of either spherical, cylindrical or lamellar domains dispersed in a continuous matrix of the other component. *Figure 1*, for example, depicts for a styrene (S)–butadiene (B) triblock copolymer either a spherical domain or the orthogonal cross-sectional view of a cylindrical domain. An interphase region, whose composition varies smoothly, extends between the domain core of S and the matrix of B. While the equilibrium morphology depends primarily on the bulk polymer composition, the phenomenon of microphase separation and the actual morphology are also functions of temperature, chemical potential, molecular weight, molecular architecture (e.g. diblock SB and triblock SBS) and formation history in general.

Microphase configurations are responsible for the material's thermomechanical properties being different from those of both homopolymers and from those of a random copolymer of equal composition[1,2]. Consequently, discerning the impact of these microstructures—quantitatively—on bulk properties is of prime concern. To this end, many investigations have relied upon bulk characterization to infer microstructural information. For example, Kraus and Rollmann[3] and Gronski *et al.*[4] have used mechanical testing to provide conclusive evidence of an interphase region existing between the microphases. In addition, their measurements of T_g^S depression offer insight into the composition of the interphase, as discussed by Henderson and Williams[5]. Attempts at directly analysing the

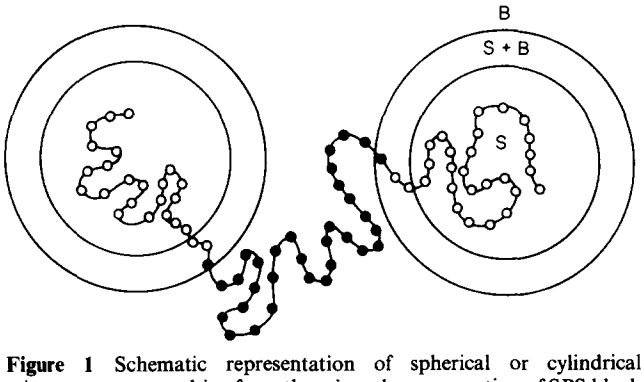

Figure 1 Schematic representation of spherical or cylindrical microstructures resulting from the microphase separation of SBS block copolymers. The domains and continuous matrix are primarily S and B, respectively, and the interphase is the mixed S + B region. In subsequent TEM analysis, only two phases (S and B) are envisioned; this essentially assigns the interphase equally to the S and B regions

0032-3861/88/030387-09$03.00

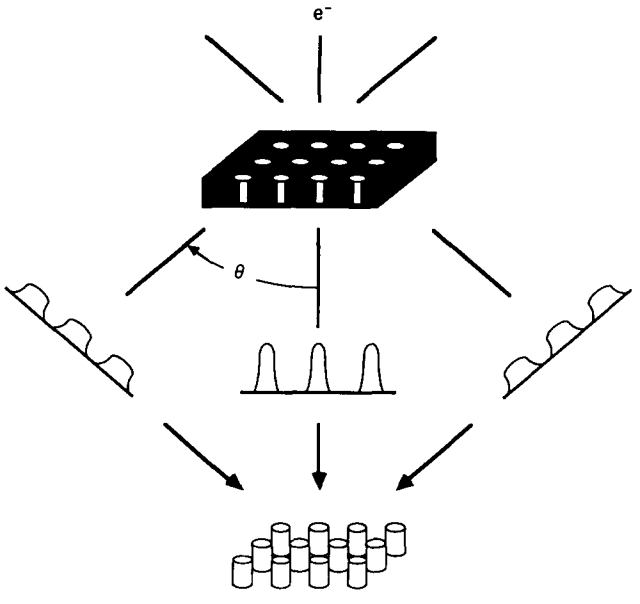

Figure 2 Representation of the back-projection method. An ultrathin-film block copolymer sample having cylindrical morphology (top) is studied with TEM at various tilt angles. Each resulting projection comprises optical densities dependent on the angle of tilt (middle). These projections are then properly summed to yield the microstructures of interest (bottom)

microstructure by using techniques such as transmission electron microscopy (TEM)[6-8], small-angle X-ray scattering (SAXS)[9-11] and small-angle neutron scattering (SANS)[12,13] have yielded information on microstructural dimensions such as the average domain size, average repeat spacing and average interphase thickness.

Complementing the experimental investigations, equilibrium thermodynamic theories have been proposed to explain the phase separation and to predict microstructural details[14-18]. All of these theories assume the presence of ideal domain geometries. The same idealization has been made in modelling linear mechanical properties in terms of the microstructure[1,3]. While it is clear that most block copolymer samples do not possess idealized microstructures, there has been virtually no effort made to examine structure–property relationships for these systems. One of the major reasons for this is the difficulty of scrutinizing the microstructure closely, as well as the subsequent steps of characterizing what is found and embedding such information in predictive models.

Here, we pursue the initial goal of directly examining non-ideal microstructures at the highly localized level of the individual domain. We have utilized TEM and a filtered back-projection method, shown schematically in *Figure 2*, to reconstruct three-dimensional images of an SBS block copolymer with cylindrical morphology. The reconstruction provides direct detailed characterization of irregular cylindrical domains and disordered domains.

EXPERIMENTAL

The block copolymer used here was an SBS manufactured and characterized by Cosden Oil and Chemical Co. (Deer Park, Texas). Having a molecular weight ($\bar{M}_w$) of 230 000 g mol^{-1} and a polydispersity ($\bar{M}_w/\bar{M}_n$) of 2.00, this sample was composed of 30 wt% polystyrene (PS) and exhibited a cylindrical morphology. Conventional TEM (roughly 60–100 kV), as was employed here, requires ultrathin sections or films less than 100 nm in thickness. In this study, a direct-casting technique described elsewhere[19] was used to produce ultrathin films less than 50 nm thick. Staining for contrast enhancement between phases was accomplished by exposure to the vapour of a 1% osmium tetroxide aqueous solution for 85 min. The sample surface was then coated with a drop of 1% aqueous polylysine, to produce a hydrophilic surface suitable for decoration with 10 nm colloidal gold particles. These particles were required as fiducial or reference markers to facilitate alignment of the micrographs (see below). Electron micrographs used in the tilt and reconstruction studies were obtained at 5° increments ranging from −60° to +50° using the goniometer of a JEOL JEM 100CX (JEOL Ltd, Peabody, Massachusetts), shown schematically in *Figure 3*, at a magnification of 33 000× and an accelerating voltage of 80 kV. Minimal beam degradation (which can be observed when it occurs) was produced in these samples over the course of the tilt study, which lasted approximately 45 min.

IMAGE ANALYSIS

Stereoscopic views

The electron micrographs, digitized using a Perkin–Elmer (Garden Grove, California) PDS microdensitometer set at a 50 μm spot size, revealed polystyrene cylinders with an average diameter of 22.8 nm and repeat distance of 42.2 nm. To facilitate stereoscopic viewing, and as a crucial prelude to calculating a three-dimensional reconstruction, alignment of the digitized images was first necessary. This corrected for any miscalibration in the goniometer stage as well as precisely determining the tilt axis within the micrographs. The

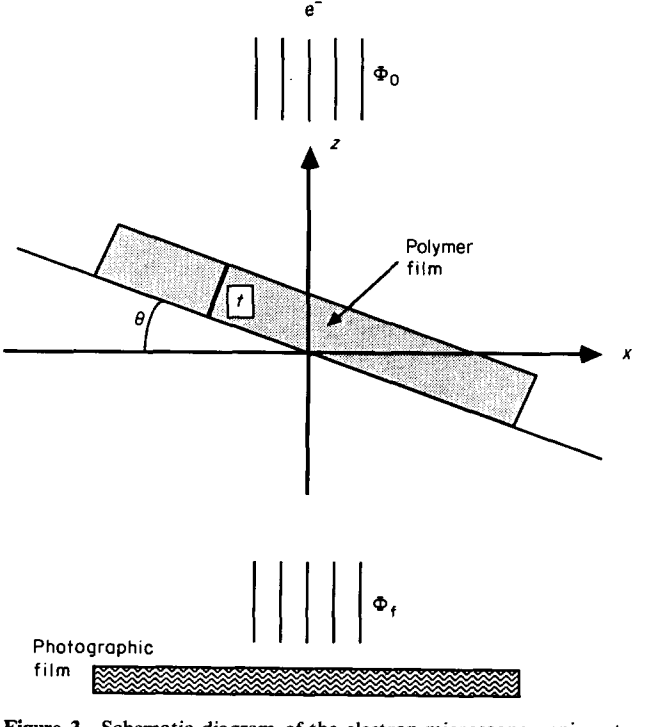

Figure 3 Schematic diagram of the electron-microscope goniometer showing the angle θ. The electron beam passes through the ultrathin film, and the resulting beam intensity (Φ_f) is recorded on photographic film

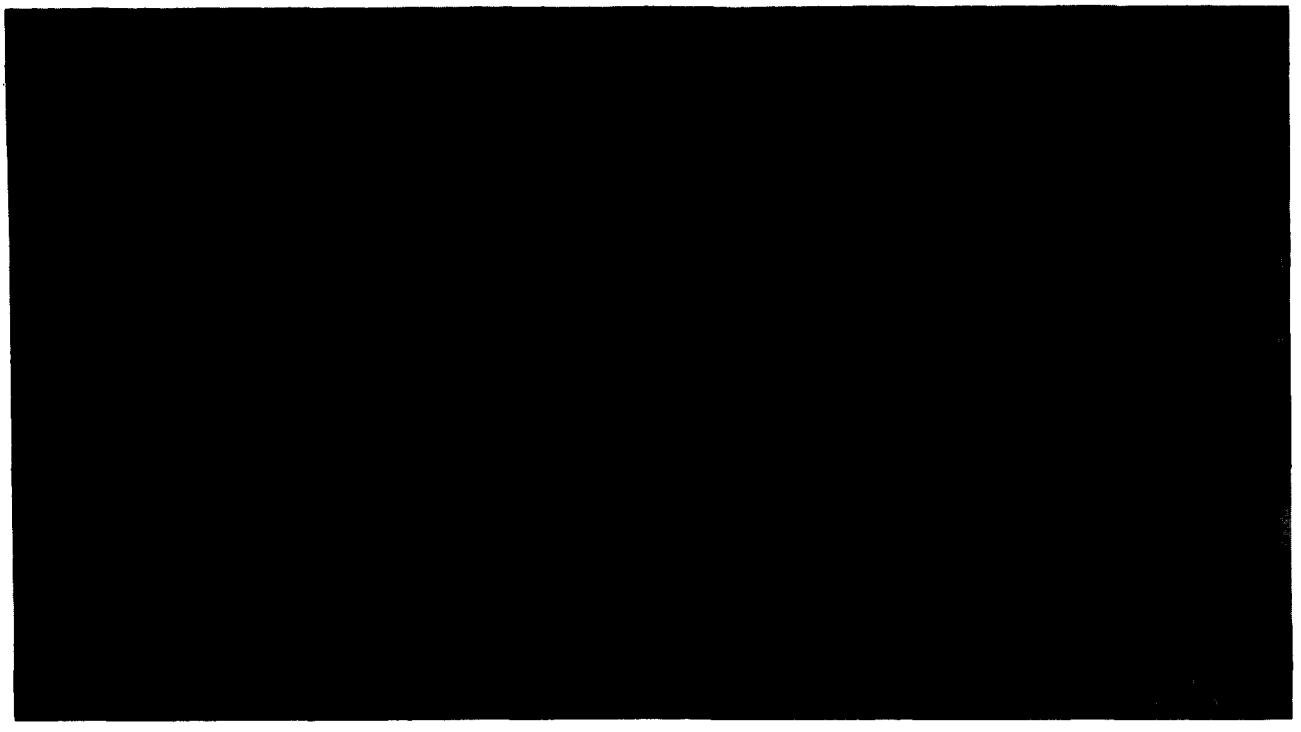

Figure 4 Stereo pair of electron micrographs with $\Delta\theta = 10°$. These micrographs were obtained at different tilt angles inside the electron microscope and were then aligned using colloidal gold fiducial markers (seen as black beads in the micrographs). When observed with a stereoscopic viewer, this pair will reveal some of the three-dimensional nature of the sample.

latter determination was non-trivial, owing to the uncontrolled and magnification-dependent rotation of the image by the electron optics within the microscope. The colloidal gold particles, shaped like spherical beads, were used as fiducial points. The necessary geometric parameters and three-dimensional coordinates of each particle were obtained by applying a least-squares conjugate gradient minimization procedure[20] to the set of 23 images*. The alignment utilized an area common to each projection in which the motions of 15 gold particles were traced as the images were tilted. Spatial orientation of the gold particles was thus obtained with an overall maximum error of 0.1% and a $-1.5°$ miscalibration was detected in the microscope goniometer. The latter shifted the range of angles from ($-60°$ to $+50°$) to ($-61.5°$ to $+48.5°$) and was later verified when the goniometer of the electron microscope was recalibrated.

Once the necessary alignment parameters were obtained, the images were corrected by biquadratic interpolation. The resultant images, each measuring 512×512 pixels, were arranged to yield stereoscopic pairs by proper alignment and separation by a relatively small angle ($\Delta\theta$). Such a pair, one of which is presented in *Figure 4* with $\Delta\theta = 10°$, can be studied with a stereoscopic viewer to acquire visually a three-dimensional portrayal of the polystyrene cylindrical domains. Upon close examination of *Figure 4* with a viewer, it is obvious that (a) not all of the domains approach the surface of the sample, (b) the well ordered cylinders appear to be oriented normal to the surface, and (c) the gold particles are lying on the upper surface of the sample.

*Two images were obtained at $-20°$, one in the forward-tilting sequence and one upon reversal, to check on the possible effects of hysteresis. There were none

Filtered back-projection reconstruction

By use of the stereoscopic pairs, it was seen that not all of the domains appeared as the idealized ones incorporated in theoretical models. Cylinders were viewed in various orientations and usually without circular cross-sections. This prompted the search for a more precise view of the cylindrical morphology in three dimensions. By methods common in medical computerized tomography, a three-dimensional reconstruction can be determined from a set of tilted projections. Several techniques have been proposed to accomplish the reconstruction[21-24]. The one chosen here was the filtered back-projection method, due to its accuracy, freedom from artifacts, and computational efficiency[24,25].

The back-projection method, in general, begins with a series of aligned images taken at different tilt angles (*Figure 2*). The images are then combined such that a three-dimensional image results from the summation of two-dimensional images. Before this can be done, however, variations in the optical densities of the tilt images (due, for example, to varying film exposure times) must be minimized. This can be done by choosing a linear scaling factor, λ, such that:

$$\lambda_k = \frac{[\sum_{i=1}^{n}\sum_{j=1}^{n}\rho^o(x_i,y_j)]_{ref}}{[\sum_{i=1}^{n}\sum_{j=1}^{n}\rho^o(x_i,y_j)]_k} \qquad (1)$$

where $\rho^0(x_i,y_j)$ is an optical-density element of the matrix ρ^0 and $n = 512$. The subscripts k and *ref* refer to images with angular tilts of θ_k and the reference orientation $\theta = 0$, respectively. To avoid skewing the linear average (i.e. the sums in eq. (1)), the low optical densities of the gold particles were removed from the averaging by defining a

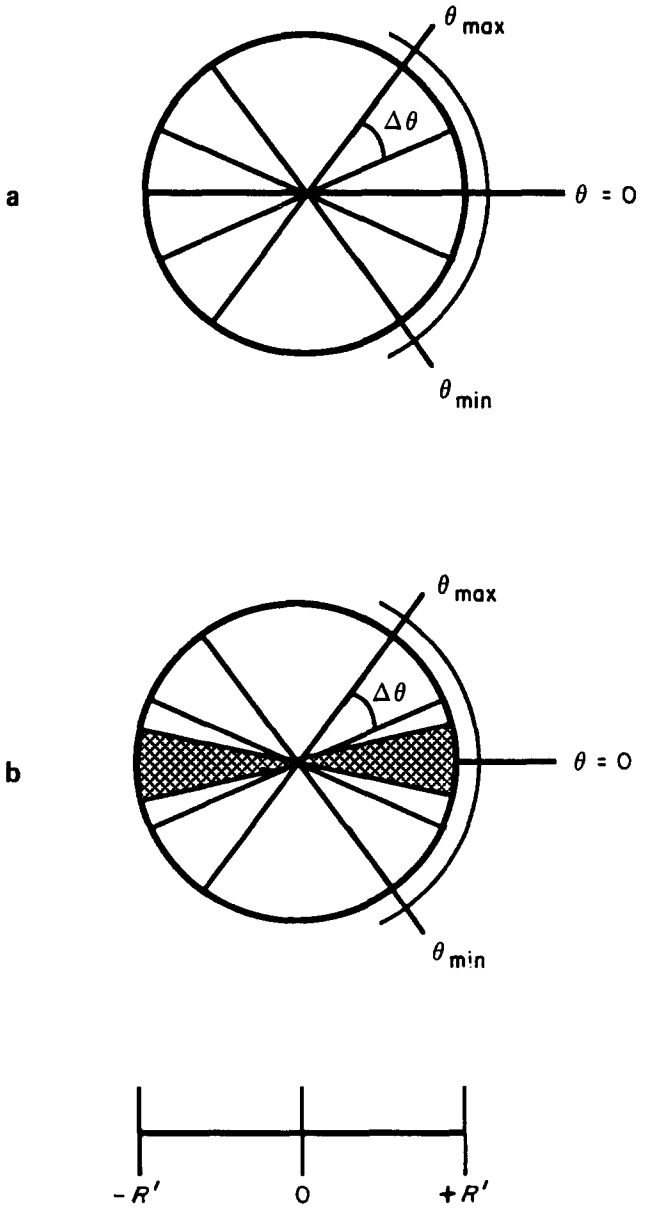

Figure 5 Principle of the back-projection reconstruction method. (a) The general method requires a series of projections at various tilt angles (θ) at increments of $\Delta\theta$; these images are then summed by aligning the single tilt axis. However, information is distorted with background noise as $\pm R'$ is approached. (b) The filtered method uses the same general technique but weights the image as a function of the radial distance r so as to obtain an accurate and undistorted representation of the solid. In this study, $\theta_{max}=48.5°$, $\theta_{min}=-61.5°$ and $\Delta\theta=5°$

density threshold below which optical densities were set equal to the average density.

Optical density as a function of film thickness and tilt is assessed[26] by assuming that film response to the electron dose is linear, giving a Beer's law relationship:

$$\rho^o(x_i,y_j,z)=\exp[-P_z(x_i,y_j)z] \tag{2}$$

where $P_z(x_i,y_j)$ is the linear absorption coefficient below a specific point (x_i,y_j) on the film surface and z is the penetration length of the beam into the sample. Optical density is evaluated at the beam exit from the sample, according to the definition $\rho^0=\Phi_f/\Phi_0$ where Φ_f is the final (exit) beam intensity and Φ_0 is the initial (entering) intensity. For a beam normal to the film surface ($\theta_k=0$), $z=t_{ij}$ (film thickness at that (x_i,y_j) position) and thus $\rho^0(x_i,y_j,t_{ij})$ is obtained. Because film thickness is essentially uniform in the present study, $t_{ij}=t$ is not a variable and the simpler function $\rho^0(x_i,y_j)$ is sufficient to describe the two-dimensional image for $\theta_k=0$. For the other θ_k, the beam path lengths t_θ are greater than $t=t_{\theta=0}$, but simple geometrical accommodations can be made. This leads to the entire set of images $\rho^0(x_i,y_j,\theta_k)$ needed for the reconstruction.

Once the optical densities are properly scaled, the series of images, all aligned with respect to the single-tilt axis (here, the y-axis), can be summed to yield a three-dimensional volume element. This method, which is the basis for back-projection reconstruction, is shown schematically as the two-dimensional representation of a cylinder in *Figure 5a*, in which each line is a projection. Use of only a finite number of projections in a simple back-projection scheme introduces a certain amount of error in the reconstruction. To minimize the effect of finite sampling and thus obtain a mathematically accurate three-dimensional representation of the specimen, the filtered (or r-weighted) back-projection method is employed, in which a spreading function operates on the image projections. This Fourier radial spreading function, $g(r)$, is indicated schematically in *Figure 5b* and obtained by:

$$g(r)=\int_{-\infty}^{+\infty} s\exp(2\pi irs)\,ds \tag{3}$$

where r is the radial distance from the tilt axis along the x-axis. The λ-scaled optical densities from the images, functions of both r and the angle of tilt, are now convolved with $g(r)$ to obtain the function $\rho'(r,y,\theta)$:

$$\rho'(r,y,\theta)=\rho^0(r,y,\theta)*g(r) \tag{4}$$

Consequently, the intensity at any point in space occupied by the specimen, $I_{x,y,z}$, is:

$$I_{x,y,z}=\sum_{k=1}^{m}\rho'(p_k,y,\theta_k) \tag{5}$$

where ρ' is given in Cartesian coordinates rather than cylindrical coordinates, m is the number of projections (23), and p_k is the kth projection along the x-axis and is determined from:

$$p_k=x\cos\theta_k+z\sin\theta_k \tag{6}$$

To acquire the complete volume element, the intensities of each projection element are summed while keeping the tilt axis properly aligned.

RESULTS AND DISCUSSION

Parallel walk

With the complete specimen volume reconstructed, we can analyse the three-dimensional features of the block copolymer microstructures. We begin our analysis by traversing the reconstruction from the top of the TEM sample to the bottom of the sample, following a path parallel to the electron beam at normal incidence. Reference is made to the sequence of views shown in

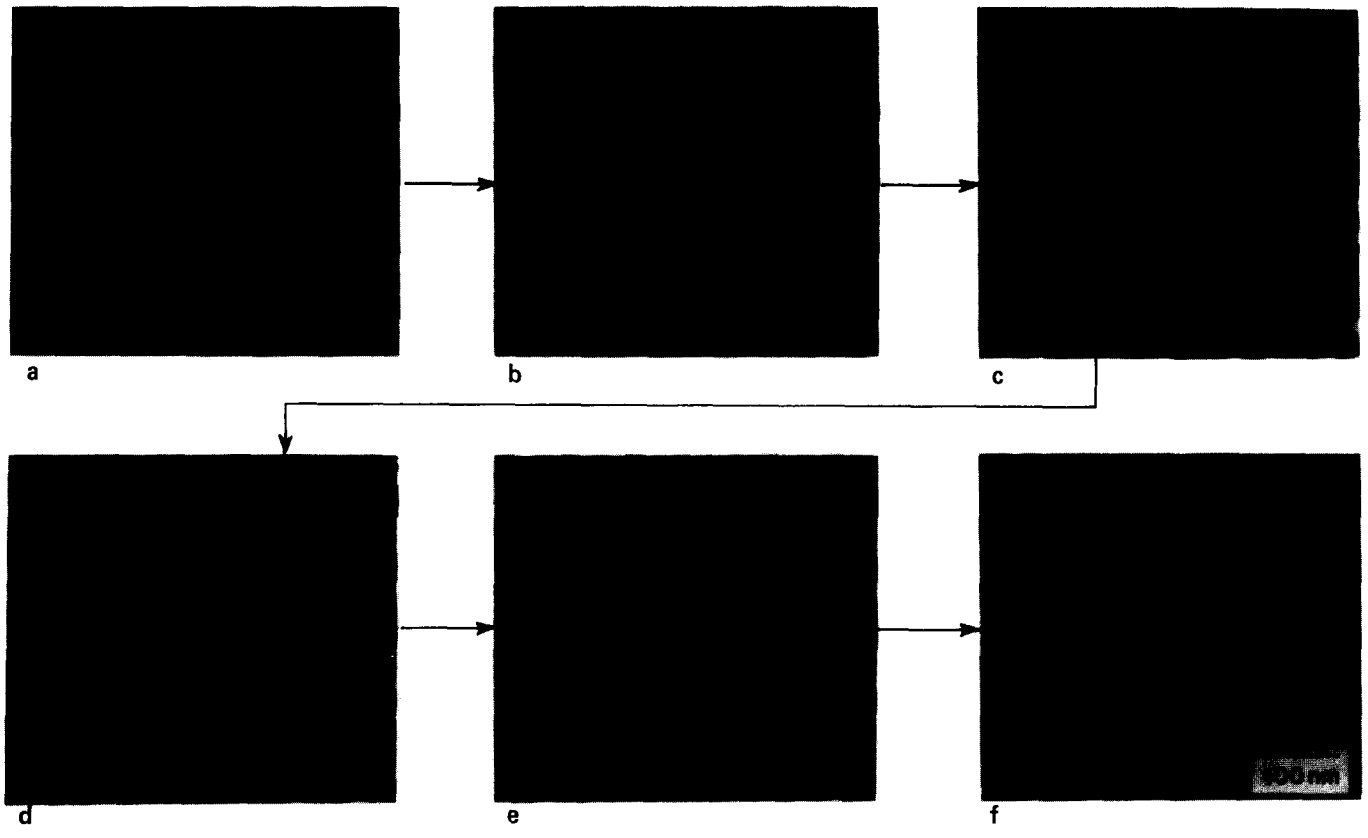

Figure 6 Serial views of walk, parallel to the electron beam, through the ultrathin film sample. Only the disc-shaped gold particles, approximately 2.5 nm thick, are in focus in (a), which thus defines the position of the film's upper surface. The upper portion of the microstructure comes into focus in (b), and the domains become increasingly prominent in (c) through (e). The sample is exited in (f). From this, the sample thickness is estimated to be approximately 36 nm

Figure 6. In the first view, only the gold beads are in sharp focus. In the next, the tops of the PS domains become distinct; and in the successive segments, the domains become fully distinguishable. In the last view, we exit through the bottom of the sample.

To characterize these cylindrical domains, we define an aspect ratio, ξ, as:

$$\xi = L/d \tag{7}$$

where L and d are the length and diameter of the cylinders, respectively. By using the known microscope magnification, some magnification–calibration grids, and the spot size of the microdensitometer, we can estimate the thickness of the sample as 36.0 nm. Since the mean diameter of the styrene structures is 22.8 nm, we expect that these domains, which extend through the sample, should appear as short, stubby cylinders (i.e. $\xi = 1.58$).

Perpendicular walk

It is also possible to examine lateral cross-sections of the sample, traversing from side to side in a plane perpendicular to the beam direction. This is shown in the contour plot of *Figure 7*. Here, the microstructures are clearly visible in this stereo pair. The aspect ratio of these plots has been increased by a factor of 10 to demonstrate better the internal detail.

Reconstruction

The ultimate objective of this work has been to reconstruct the polystyrene microstructures in three dimensions. The degree of image detail revealed in the reconstruction is, to some extent, governed by the intensity contour level employed. We elected to suppress interphase effects, in favour of highlighting whole-domain clusters. By selecting an intensity contour level such that the domain repeat distance agreed with previous studies[19], we discriminated among the volume-element intensities, $I_{x,y,z}$, and used a shading program devised to obtain the reconstructions presented in *Figures 8* and *9*. In *Figure 8a*, we see a group of stubby cylinders ordered in close-to-hexagonal packing. Clearly, though, the cylinders are not ideal and exhibit variations in both thicknesses and geometry. In fact, some of the cylinders, though separated for the most part, are actually connected near their lower bases. (Locations of the sample top and bottom were derived from calculations of the gold-bead thickness and the parallel walk.) The uniformly flat upper surfaces of the cylinders correspond to the calculated top surface of the polymer film, demonstrating that the cylinders do indeed extend from top to bottom of the ultrathin film. The fact that cylinder heights are equal to the film thickness eliminates the possibility that an upper layer of polybutadiene shields the polystyrene cores of the cylinders. A similar conclusion was reached by Thomas and O'Malley[27,28] using X-ray photoelectron spectroscopy in the study of polystyrene/poly(ethylene oxide) diblock and triblock copolymer surfaces. In addition, *Figures 8a* and *8b* demonstrate that these cylinders are oriented normal to the sample surface. Despite the many deviations from ideality, the microstructure displayed in *Figure 8* and those in several other cases agree quite well in many

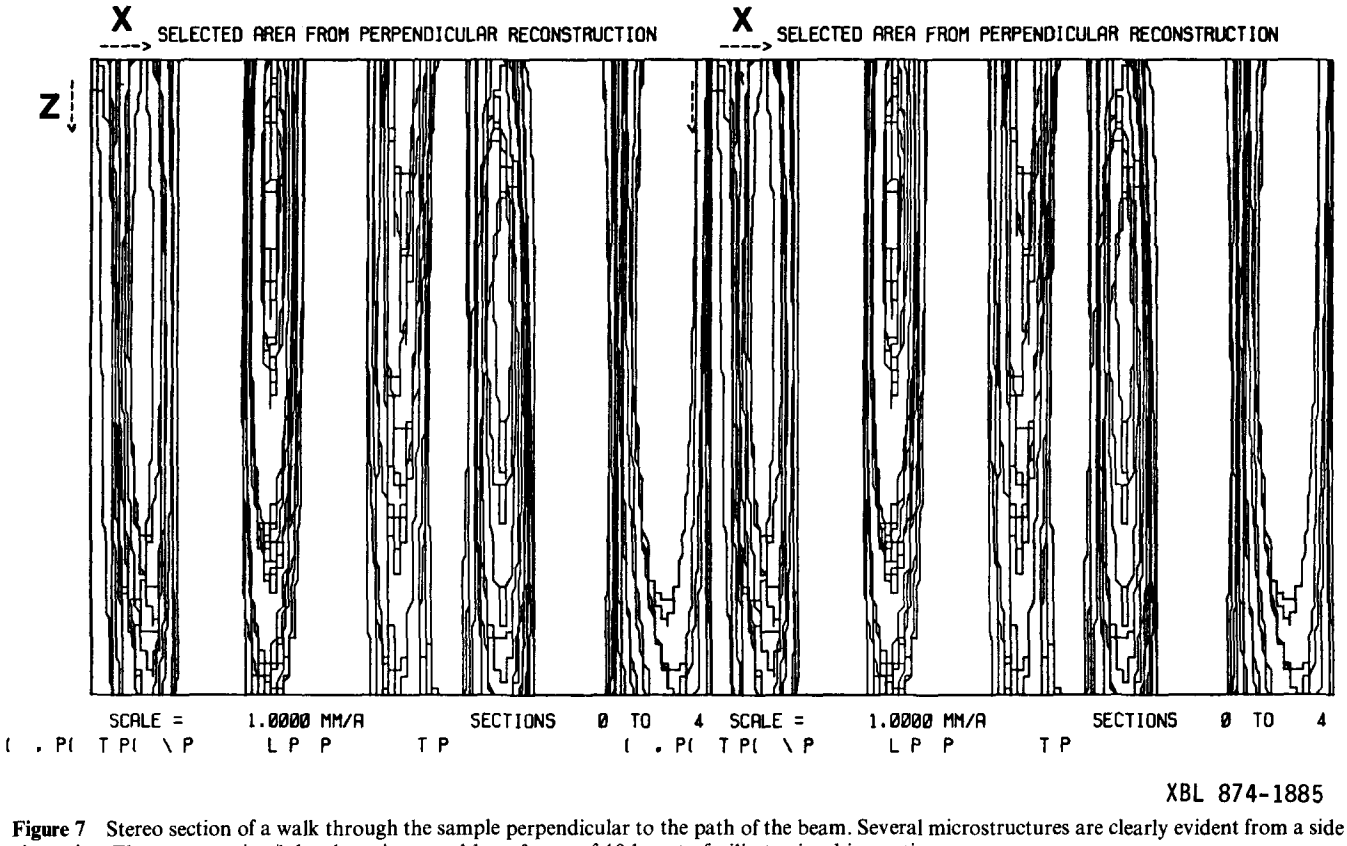

Figure 7 Stereo section of a walk through the sample perpendicular to the path of the beam. Several microstructures are clearly evident from a side viewpoint. The aspect ratio, ξ, has been increased by a factor of 10 here to facilitate visual inspection

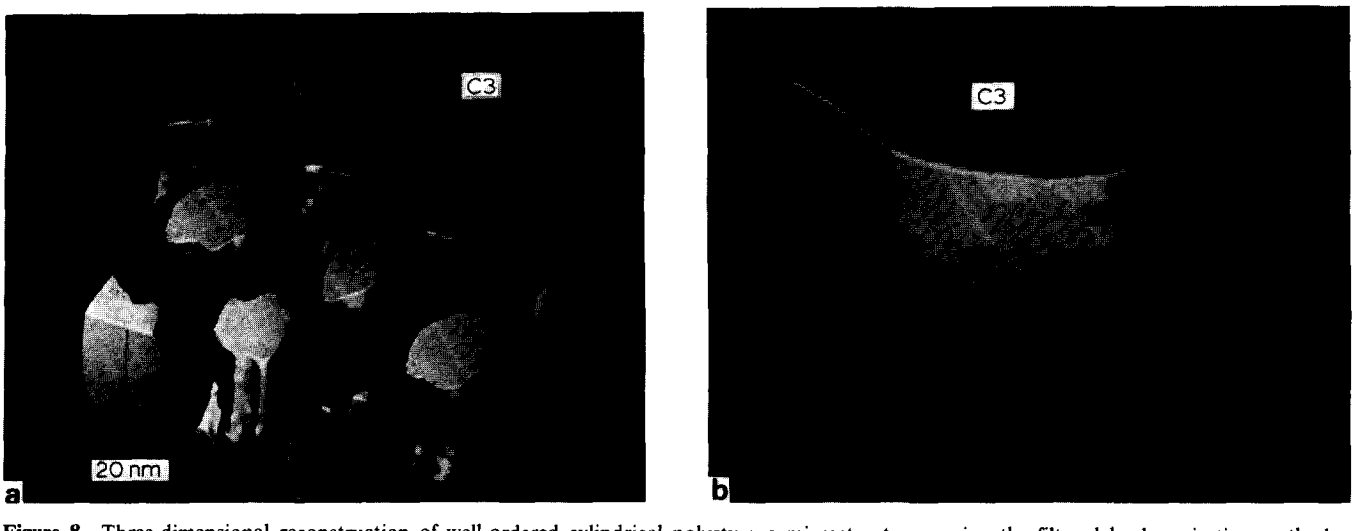

Figure 8 Three-dimensional reconstruction of well-ordered cylindrical polystyrene microstructures, using the filtered back-projection method. Hexagonal packing prevails in (a), in which the cylinders exhibit two important characteristics: (1) they extend throughout the thickness of the sample (note the flat upper and lower surfaces) and (2) they are oriented normal to the surface. Cylinder C3, rotated to present another view, is shown in greater detail in (b)

quantitative respects (average domain diameter, repeat spacing, hexagonal packing, local alignment, etc.) with predictions made by equilibrium theory.

In *Figure 9*, however, we see microstructural elements that have certainly not achieved an equilibrium state. Even though the solvent used for casting the film specimens (toluene) is preferentially good for polystyrene, and thus is believed to be localized in the domain[29] if remaining at all, we have no reason to believe that a significant degree of solvent swelling of the domains is responsible for this localized non-equilibrium state. Other factors, based on the polymer itself, have sometimes been associated with this condition. One investigation[30] has concluded that, the longer the polymer chain, the greater the probability that it will be trapped in a non-equilibrium state due to limitations in diffusional mobility during the phase-transformation process. This observation, coupled with the results of a study showing that molecular weight polydispersity also affects polymer diffusion[31], suggests that the copolymer studied here ($\bar{M}_w = 230\,000\ \mathrm{g\ mol^{-1}}$ and $\bar{M}_w/\bar{M}_n = 2.00$) will exhibit some non-equilibrated microstructures. In addition, Hadziioannou and Skoulios[32] investigated the effects of polydispersity on block copolymer microstructural dimensions. They mixed polystyrene/polyisoprene diblock and triblock copolymers of varying molecular

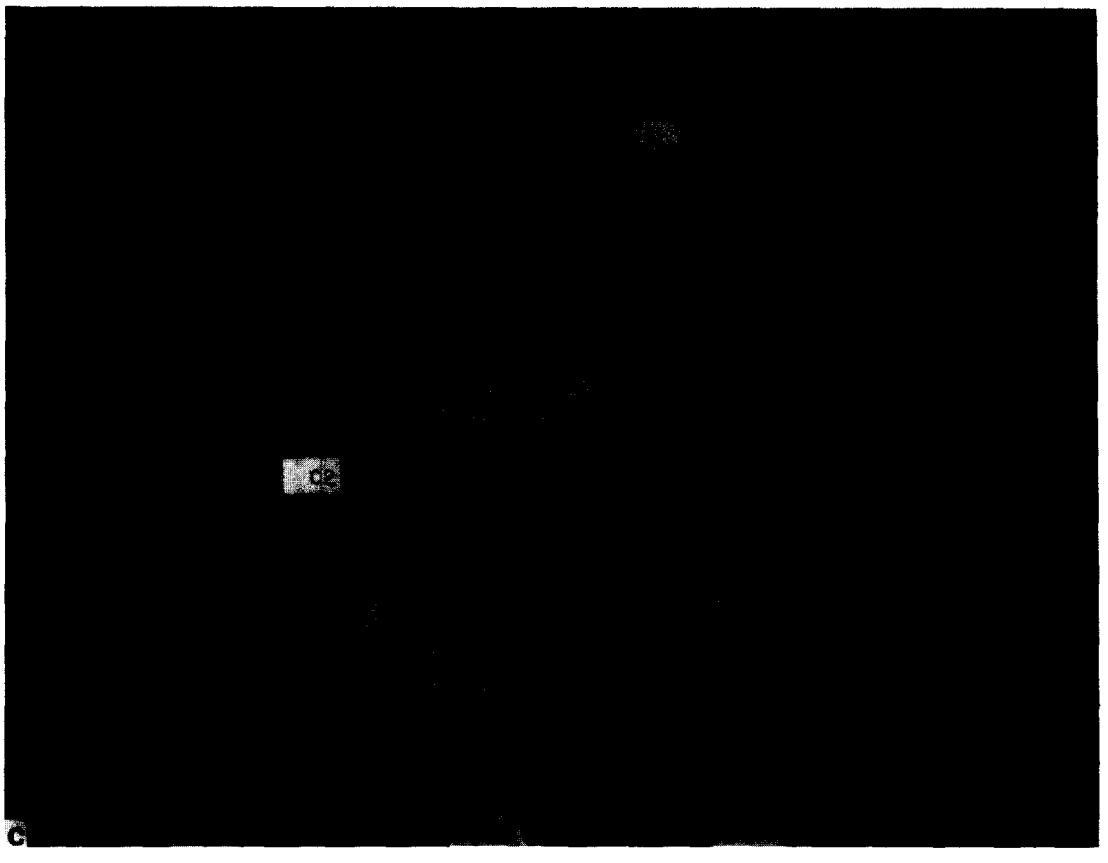

Figure 9 Three-dimensional reconstruction of some non-equilibrated polystyrene domains resembling globules. This condition provides useful information regarding evolution of the microphase separation. Here, aggregate C1 resembles a prolate ellipsoid, a structure intermediate between a sphere and a cylinder. This implies that spheres form first and then evolve into cylinders. Further evidence of this behaviour is seen in globules labelled C2. These resemble cylinders but retain some ellipsoidal curvature

weights and found that the repeat distance tends to decrease, for the most part, with increasing $\bar{M}_w/M_n$. A similar trend is predicted to occur with blends of pure diblocks and with blends of pure triblocks, the effect being much more pronounced for diblocks than for triblocks[33]. Moreover, the report[34] that polydisperse polyurethanes exhibit fatigue earlier than nominally monodisperse samples may signal the presence of 'defective' microstructures (as in *Figure 9*) in the former.

The non-equilibrium structures found in *Figure 9* may also present some clues as to the evolution of microstructure formation. For example, the aggregate labelled C1 is clearly a prolate ellipsoid not touching the top or bottom of the TEM sample film. This implies that (a) the domain, when solidified, possessed a shape intermediate between a sphere and a cylinder and (b) the system prefers to have polybutadiene blocks above and below the domain, at the sample surfaces. This latter point suggests that the overall free energy of a finite system—e.g. a thin film—is initially minimized when polystyrene spherical domains form at positions far from any surfaces, with the air/polymer interface being the low-energy polybutadiene one. This point has been addressed elsewhere[35]. However, as phase separation continues and more of the polystyrene phase appears, the spheres give rise to cylinders. This process is represented schematically in *Figure 10*. There, the intermediate stage of the prolate ellipsoid is also shown, at a point where the top of the domain has already reached the film surface and become flattened; this resembles the aggregates labelled C2 in *Figure 9*. The evolution shown in *Figure 10* requires some complex rearrangements of chains in the original sphere and also in subsequent stages of the changing ellipsoid. It seems likely that some polybutadiene chains are thereby trapped within newly developing portions of the polystyrene core, their escape hindered by diffusive limitations and possibly prevented entirely as the polystyrene becomes glassy. This might account for the geometrical imperfections in cylindrical domains (*Figure 8*) as well as abundant evidence[1,36] that polystyrene phases in styrene/rubber block copolymers contain residual rubber. This kinetics argument is even more persuasive in view of the recent theoretical result[37] that no microstructural system seems capable of a thermodynamic equilibrium wherein rubber remains in the polystyrene core.

There are other important implications from the evolutionary sequence proposed above for domain formation. One is that kinetic limitations may play a major role in determining the fundamental *shape* of domains detected at a later time (i.e. spheres vs. cylinders) and not only the degree of perfection of that shape. Another implication is that some sort of epitaxial process of phase growth may prevail in certain circumstances, such as a spherical 'seed' generating a cylinder growing with the same diameter (perhaps even if the cylinder is not the true equilibrium morphology). This phenomenon has already been reported[38,39] in another block system, a poly(styrene-*b*-4-vinylpyridine), which had a lamellar microstructure at equilibrium. When this polymer was

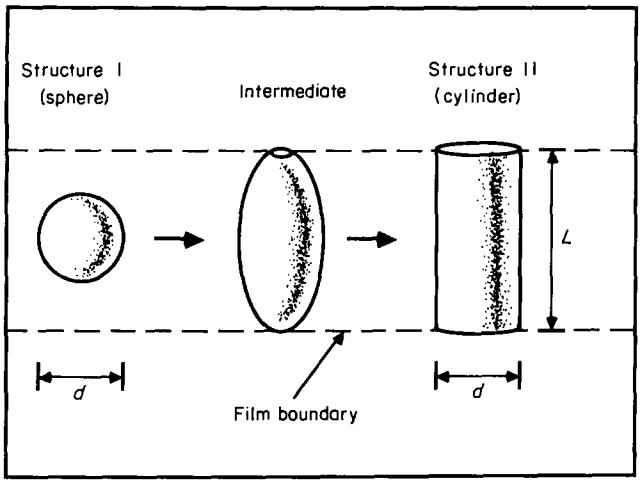

Figure 10 Schematic representation of possible block copolymer microstructure evolution from spherical to cylindrical morphology; the diameter size scale (d) seems to be maintained throughout the process. The cylinder length, L, in this case is equal to the film thickness t. Only ultrathin films, approximately on the size scale of the microstructures themselves, are considered here

cast upon another block copolymer having spherical styrene domains, the latter initiated growth of styrene cylinders in the former, with the cylinders having the same diameters as the template spheres. This process, termed 'epitaxy in mesophases' by the authors[38,39], may be more widespread than previously recognized.

The ability to reconstruct complex three-dimensional structures from a series of TEM images taken at different tilt angles is a general one and can be used in the study of a wide variety of materials, including biological specimens[40]. Specimen thickness is limited by the electron microscope's chromatic aberration and depth of focus. The use of higher electron acceleration energies allows specimens substantially thicker than those reported here to be examined. Current-generation intermediate-voltage transmission electron microscopes (300–400 kV) provide a nearly ideal combination of properties for studying materials up to 0.75 μm thick.

The resolution limit of the reconstruction is a function of the number of tilted views, the dynamic range and signal-to-noise properties of the recording media. Direct digital data collection using large-area cooled CCD (charge-coupled device) arrays in conjunction with automated high-tilt goniometer stages should allow for nearly effortless high-resolution three-dimensional data collection from semi-thick specimens. Such approaches are currently being developed for biological studies[41].

CONCLUSIONS

In this study, we have used TEM tomographic imaging to scrutinize in three-dimensional detail the cylindrical polystyrene domains of a microphase-separated SBS block copolymer. Micrographs of the copolymer were acquired at various angles of tilt with the goniometer of the electron microscope. Alignment of 23 images, each separated by 5°, resulted in stereoscopic pairs which produced three-dimensional images when observed with a stereoscopic viewer. Such images showed that (a) some of the domains in the sample did not extend to the surface, though most did, and (b) some of the microstructures were not normal to the surface, though most were.

After the 23 projections were scaled with respect to average optical density and angular variations, a filtered back-projection method was used to reconstruct the polystyrene domains in three dimensions. Two categories of structures were observed. The first was a well-ordered group of cylindrical domains distributed on a hexagonal lattice, with average diameters of approximately 23 nm. Cross-sections of the cylinders exhibited irregular deviations from circularity. These cylinders were oriented normal to the surfaces of the ultrathin film and extended throughout the thickness of the sample (approximately 36 nm). In the second category, domains exhibited non-equilibrium characteristics and appeared as irregular globules. Trends of microstructural evolution were inferred from a reconstruction showing a non-equilibrated globular grouping and may help to explain 'epitaxy in mesophases' evident in other work. The role of such aggregates in determining the bulk properties of microphase-separated block copolymers remains to be established.

ACKNOWLEDGEMENTS

The authors would like to thank D. Kelly of Cosden Oil and Chemical Co. for the block copolymer sample, C. Schooley and the staff of the Electron Microscope Laboratory (University of California, Berkeley) for guidance in TEM operations, K. Downing (Lawrence Berkeley Laboratory) for help in the image digitizing, and E. Sheena of the Computer Service Facility (Lawrence Berkeley Laboratory) for consultation. This work was supported by the Director, Office of Energy Research, Office of Basic Energy Sciences, Materials Science Division of the US Department of Energy under Contract No. DE-AC03-76SF00098.

REFERENCES

1 Diamant, J., Ph.D. Thesis, University of California, Berkeley, 1982
2 Hashimoto, T., Tsukahara, Y., Tachi, K. and Kawai, H. *Macromolecules* 1983, **16**, 648
3 Kraus, G. and Rollmann, K. W. *J. Polym. Sci., Polym. Phys. Edn.* 1976, **14**, 1133
4 Gronski, W., Annighofer, F. and Stadler, R. *Makromol. Chem., Suppl.* 1984, **6**, 141
5 Henderson, C. P. and Williams, M. C. *Polymer* 1985, **26**, 2021
6 Annighofer, F. and Gronski, W. *Makromol. Chem.* 1984, **185**, 2213
7 Spontak, R. J., Williams, M. C. and Schooley, C. N. *J. Mater. Sci.* 1986, **21**, 3173
8 Spontak, R. J., Agard, D. A. and Williams, M. C. *Macromolecules* in press
9 Richards, R. W. and Thomason, J. L. *Polymer* 1983, **24**, 1089
10 Richards, R. W. and Thomason, J. L. *Polymer* 1981, **22**, 581
11 Leung, L. M. and Koberstein, J. T. *Macromolecules* 1986, **19**, 706
12 Mayer, R. *Polymer* 1974, **15**, 137
13 Hashimoto, T., Fujimura, M. and Kawai, H. *Macromolecules* 1980, **13**, 1660
14 Leary, D. F. and Williams, M. C. *J. Polym. Sci., Polym. Phys. Edn.* 1973, **11**, 345
15 Henderson, C. P. and Williams, M. C. *J. Polym. Sci., Polym. Phys. Edn.* 1985, **23**, 1001
16 Meier, D. J. *ACS Polym. Prepr.* 1974, **15**(1), 171

17 Helfand, E. *Macromolecules* 1975, **8**, 552
18 Helfand, E. and Wassermann, Z. R. *Macromolecules* 1976, **9**, 879; 1978, **11**, 960; 1980, **13**, 994
19 Spontak, R. J. in 'Proceedings of the 44th Annual Meeting of the Electron Microscopy Society of America' (Ed. G. W. Bailey), San Francisco Press, San Francisco, 1986, p. 788
20 Lawrence, M. C. *Electron Microsc. Soc. S. Afr. Proc.* 1983, **13**, 19
21 Gorden, R. *Int. Rev. Cytol.* 1974, **38**, 111
22 DeRosier, D. J. and Klug, A. *Nature* 1968, **217**, 130
23 Ramachandran, G. N. and Lakshminarayanan, A. V. *Proc. Nat. Acad. Sci. USA* 1971, **68**, 2236
24 Muehllehner, G. and Wetzel, R. A. *J. Nucl. Med.* 1971, **12**, 76
25 Morgan, C. L. 'Basic Principles of Computer Tomography', University Park Press, Baltimore, 1983, Ch. 5
26 Grum, F. and Becherer, R. J. 'Optical Radiation Measurements: Radiometry', Academic Press, New York, 1979, pp. 21–3
27 Thomas, H. R. and O'Malley, J. J. *Macromolecules* 1979, **12**, 323
28 Thomas, H. R. and O'Malley, J. J. *Macromolecules* 1979, **12**, 996
29 Douy, A. and Gallot, B. *Makromol. Chem.* 1972, **156**, 81
30 Kinning, D. J. and Thomas, E. L. *Macromolecules* 1984, **17**, 1712
31 Mills, P. J., Green, P. F., Palmstrom, C. J., Mayer, J. N. and Kramer, E. J. *J. Polym. Sci., Polym. Phys. Edn.* 1986, **24**, 1
32 Hadziioannou, G. and Skoulios, A. *Macromolecules* 1982, **15**, 267
33 Spontak, R. J. PhD Thesis, University of California, Berkeley, 1987
34 Lin, S. B., Hwang, K. K. S., Wu, K. S., Tsay, S. Y. and Cooper, S. L. *Polym. Mater. Sci. Eng.* 1983, **49**, 53
35 Pekala, R. W. and Merrill, E. W. *J. Colloid Interface Sci.* 1984, **101**, 120
36 Diamant, J., Soong, D. S. and Williams, M. C. in 'Contemporary Topics in Polymer Science' (Eds. W. J. Bailey and T. Tsurata), Plenum Press, New York, 1984, Vol. 4, p. 599
37 Henderson, C. P. and Williams, M. C. *Polymer* 1985, **26**, 2026
38 Ishizu, K., Hayashi, T. and Fukutomi, T. *Makromol. Chem.* 1986, **187**, 689
39 Ishizu, K. and Fukutomi, T. *Makromol. Chem., Rapid Commun.* 1986, **7**, 505
40 Belmont, A. and Agard, D. A. *J. Cell Biol.* 1987, **105**, 77
41 Agard, D. A. and Sedat, J. W., work in progress, 1987